JGR Oceans

RESEARCH ARTICLE
10.1029/2019JC016031

A Spectrally Consistent Globally Defined Geodetic Mean Dynamic Ocean Topography

Frank Siegismund[1]

[1]Inst. Astr. & Phys.Geodesy, Technische Universität München, Munich, Germany

Key Points:

- The proposed methodology for land filling the mean sea surface (MSS) strongly reduces Gibbs effects in the mean dynamic topography (MDT)
- Recent geoid models contain physical information at least up to maximum degree and order (d/o) 420 corresponding to 48-km length scale

Correspondence to:
F. Siegismund,
frank.siegismund@tum.de

Citation:
Siegismund, F. (2020). A spectrally consistent globally defined geodetic mean dynamic ocean topography. *Journal of Geophysical Research: Oceans*, *125*, e2019JC016031. https://doi.org/10.1029/2019JC016031

Received 27 DEC 2019
Accepted 23 JUN 2020
Accepted article online 3 JUL 2020

The copyright line for this article was changed on 21 AUG 2020 after original online publication.

Abstract The space-borne geodetic temporal mean dynamic topography (MDT) is obtained from the difference of altimetric mean sea surface (MSS) h and the geoid height N. With the geostrophic surface currents obtained from its gradient, the MDT is an essential parameter when describing the ocean dynamics. Spectral consistency of h and N is crucial to minimize MDT errors. Frequently, h is globalized to allow for a spherical harmonic analysis, and small scales beyond maximum degree and order (d/o) resolved in the geoid are cut off. However, common globalization causes ocean-land steps in $h - N$ and spectral inconsistencies of N and h over land. To overcome both issues, a methodology is proposed based on globalization of the MDT. A Laplacian smoother with the coastal MDT values as boundary condition is applied, resulting in a smooth surface over land and a continuous ocean-land transition. The new methodology strongly reduces Gibbs effects and the need to work with high-resolution MDTs to minimize them. Reduction of resolution is tested to reduce MDT uncertainties caused by the commission error expected to increase with decreasing scale. Applying drifter data and a high-resolution hydrodynamic ocean model, it is shown that for the Gulf Stream and the Kuroshio, geodetic MDTs applying recent combined geoid models contain physical information up to at least d/o 420 (48-km spatial scale). For oceanic regions with strong geoid gradients, a higher-resolution MDT might be needed to prevent Gibbs effects caused by remaining inconsistencies between the geoid and the MSS.

1. Introduction

The ocean dynamic topography (DT) is an essential parameter in oceanography. It is defined as the deviation of the geometrical ocean surface from the geoid, which itself is the equipotential surface of gravity closest to the ocean surface in a least-squares sense. Defined like this, the geostrophic surface currents follow the isolines of the DT and their strength is determined from the gradient of the DT and the local Coriolis parameter. The geostrophic currents are the equilibrium of horizontal pressure gradient and Coriolis force and quite accurately describe the circulation on large spatial (>1,000 km) and temporal (few days and longer) scales.

Applying space-borne observations, global maps of the temporal mean DT (MDT) can be determined as the difference of the temporal mean geometric surface of the ocean h observed from altimetry and the geoid N obtained from gravity measurements. This observation strategy is very powerful, providing global maps of a useful parameter for oceanography that can hardly be obtained by other means. In recent years, the U.S./German GRACE (Tapley et al., 2004), recently extended by its Follow-On, and the ESA GOCE (Rummel et al., 2002) satellite missions have provided high-precision gravimetric measurements with respective improvements in the accuracy of gravity-based geoids. Satellite-only geoid models are now available up to degree and order (d/o) 300, corresponding to 67-km spatial resolution. Combined geoid models in addition utilize altimetry data and terrestrial gravity data up to a $5' \times 5'$ grid, which corresponds/results in gravity field models and geoids up to approximately d/o 2,160 (or approximately 9-km spatial scale).

The computation of the MDT as the difference of h and N, however, is a challenging task since this difference is two orders of magnitude smaller than the two almost identical parameters. In addition, observation strategies and physical nature of the two quantities differ. h is observed as a geometrical quantity and naturally provided on an ocean-only grid, whereas the geoid is a global linear functional of the Earth's gravity potential provided usually in spectral space as Stokes coefficients which result from projecting the potential onto spherical harmonic (SH) functions. The small deviation between h and N compared with the larger spatial variations of the geoid is not limited to low d/o coefficients. Also, on small spatial scales, spectral power in N is of comparable or higher magnitude compared with the MDT. This makes spectral consistency of N and h over a wide range of spatial scales a central issue for the quality of the resulting MDT.

A common strategy for a spectrally consistent combination of h and N to obtain the MDT is the spectral approach as described by Bingham et al. (2008). Here h has to be globalized which needs a filling in of land values. Then, spectral consistency is established by performing an SH analysis, then cutting off the Stokes coefficients for SH functions above maximum d/o n of the applied geoid model and finally synthesizing back to a desired grid in physical space. Subtraction of N from the globalized and filtered h_n provides the MDT that is finally spatially filtered if needed.

For the necessary filling in of land data, usually geoid height from a specific geopotential model is applied. Either the mean sea surface (MSS) is already provided as global field by the producer and is used unchanged (Knudsen et al., 2011; Sanchez-Reales et al., 2013) or that geoid model is applied which is later also subtracted from the MSS to obtain the MDT (Feng et al., 2013; Sanchez-Reales et al., 2016). Though this filling in with geoid data is very convenient, it causes two sources of errors when subsequently applying the spectral filter to the globalized MSS:

1. an ocean-land step is inevitable since the MSS is the sum of geoid and MDT, while over land, only geoid height is set, and
2. the geoid data used for land fill in are usually spectrally inconsistent with the geoid contained in the MSS over the ocean.

Both issues will cause unphysical wave patterns that spread into the ocean when a spectral cut-off filter is applied. This noise is increasing with decreasing cut-off d/o. The unavoidable distortion of the spectral content of a globalized MSS in the described way is concluded in Albertella and Rummel (2009) based on an idealized 1D example. To avoid this distortion, both issues, the ocean-land step and the spectral inconsistency of land and ocean geoid, are tackled in this paper, applying an easy to implement approach. The fundamental idea is to understand the MDT as a global field and to define land values as function of the coastal ocean values with the objective to minimize unphysical signals over the ocean when (spectral) filtering is applied. Though it is not claimed that the objective is fulfilled completely, it is shown that the proposed approach solves the dominant ocean-land step problem and strongly reduces unphysical wave patterns in low-resolution MDT solutions.

An assessment of geodetic MDTs applying a conventional MSS globalization approach has been provided in Siegismund (2013). There, geostrophic surface currents obtained from the MDTs have been compared with near-surface drifter data. With the proposed new approach, it is shown here that the comparison strongly improves.

Besides the globalization of h, still following the spectral approach (Bingham et al., 2008), the cut-off maximum d/o of the MDT has to be selected. So far, this selection is dominated by the mentioned wave patterns of Gibbs effects caused by the inability to reproduce the ocean-land step with limited spatial resolution, which increases with decreasing maximum d/o and is the dominant error component in low-resolution MDTs. Thus, high resolution is needed, though both the commission error in geoid and the MSS are expected to increase with decreasing spatial scale and it is not known up to which resolution the geodetic MDT actually contains physical information.

The proposed globalization strategy for h results in a substantial reduction of noise in low-resolution MDT solutions. Thereby, the trade-off of increasing commission and decreasing omission error with increasing spectral resolution comes into focus when selecting the maximum d/o of the dedicated MDT. To provide useful information about signal content in the small scales of recent geoid models is thus the second subject of this paper. This issue is interesting by itself and will facilitate the appropriate choice of the cut-off d/o in practical applications.

The remainder of the paper is organized as follows: in section 2, the general methodology to compute an MDT and the applied models for h and N are introduced. For the assessment of surface geostrophic currents obtained from the MDTs, we compare with both near-surface drifter data and results from a high-resolution hydrodynamic ocean model of the North Atlantic. Both tools are explained in this section. In section 3, the methodology for globalizing the MSS is introduced. The MDTs and geostrophic surface currents derived by this approach are assessed by comparison with other commonly used methods. Section 4 is dedicated to small-scale signal content in MDTs derived by applying recent high-resolution combined geoid models. It is investigated to what extent the geostrophic surface currents of small-scale currents are reproduced

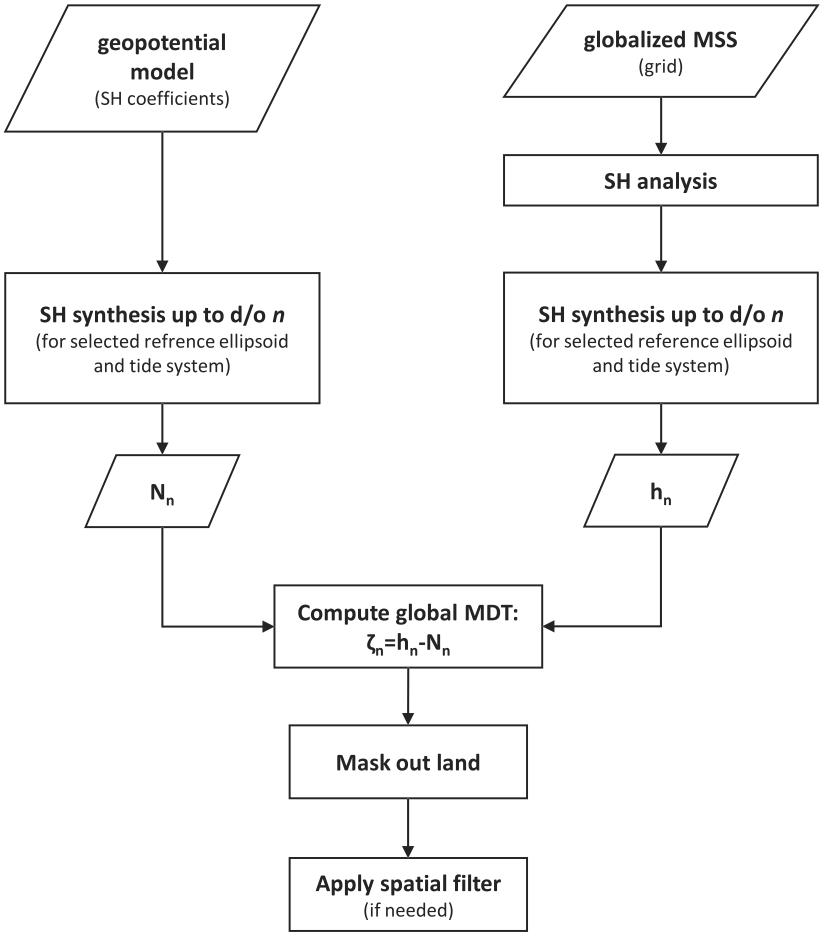

Figure 1. Workflow for the computation of MDTs.

depending on the resolution of the MDTs. For this issue, the Gulf Stream and the Kuroshio are selected since here the resolution down to small scales is needed to resolve the full current due to the short across-scale of the currents. In addition, the uncertainty in currents caused by the commission error in both the MSS and the geoid has as low as possible weight due to the large signal strength. In section 5, the results are discussed and conclusions given.

2. Methodology and Approach

2.1. Mean Dynamic Topography

The geodetic MDTs in this paper are computed as deviation of the MSS from the geoid model. The methodology is illustrated in the workflow presented in Figure 1. Both MSS and geoid model use the same tide system (tide free) and reference ellipsoid (TOPEX). The methodology then follows the spectral approach as described in Bingham et al. (2008). In this approach, the globalized MSS model is spectrally filtered to a maximum d/o. The filter consists of a projection to SH functions and a subsequent synthesis back to a gridded function applying only those SH coefficients smaller or equal to a cut-off maximum d/o n selected for the MDT. The spectral filter is termed f_n in the following. A detailed description is provided in Bingham et al. (2008). Then, the geoid is synthesized to the same maximum d/o and grid and subtracted from the MSS. The resulting MDT is spatially filtered if necessary.

For the MSS, we use DTU15 (Andersen et al., 2016). The correction of the land values in this already globalized model is a central subject of this paper and explained and assessed in section 3.

Table 1
Gravity Field Models Applied to Obtain the Geoid Height

Model	Data	Degree	Reference
TIM_R6	S(GOCE)	300	Brockmann et al. (2014)
XGM2016	A,G,S(GOCO05s)	719	Pail et al. (2018)
GOCO05c	A,G,S	720	Fecher et al. (2017)
SGG-UGM-1	EGM2008, S(GOCE)	2,159	Liang et al. (2018)
GECO	EGM2008, S(GOCE)	2,190	Gilardoni et al. (2016)
EIGEN6C4	A,G,S(GOCE), S(GRACE), S(Lageos)	2,190	Förste et al. (2014)
EGM2008	A,G,S(GRACE)	2,190	Pavlis et al. (2012)

Note. In the data column, the data sets used in the development of the models are summarized, where S is for satellite (e.g., GRACE, GOCE, Lageos), A is for altimetry, and G for ground data (e.g., terrestrial, ship-borne, and air-borne measurements). If available gravity field models are applied, this is also indicated (e.g., GOCO05s, EGM2008).

The geoid models we apply to compute the different MDTs are listed in Table 1. They are obtained from recent gravity field models available for download at the International Centre for Global Earth Models (ICGEM). For the combined models, the newest releases from the different processing centers are chosen. In addition, TIM_R6 (Brockmann et al., 2014) is selected as a recent satellite-only model.

The MDTs are computed on a $10' \times 10'$ grid. Spatially filtered MDTs are needed and obtained, by applying a truncated Gaussian kernel. Only values within a radius of three times the selected filter length around the target point are taken into account to compute the filtered value. To consider only ocean values, a land-sea mask is applied, before the filtering is performed.

The effects of the proposed methodology for land filling the MSS are largest for low-resolution MDTs. In addition, satellite-only models, specifically including GOCE mission data, have been used frequently in recent years for computing geodetic MDTs. Therefore, the low-resolution GOCE geoid model (TIM_R6) is used in section 3 to obtain the MDTs applying and comparing different methods for land filling the MSS. The GECO model is used to calculate coastal MDT values needed for MSS land filling with the new methodology explained in section 3, though the other three very high resolution models (SGG-UGM-1, EIGEN6C4, and EGM2008) were also tested and show similar results. All combination models are used in section 4 for the investigation of MDT small-scale signal content.

With local Cartesian coordinates x and y towards east and north, respectively, the zonal (meridional) geostrophic surface currents u (v) are calculated from the MDTs as

$$u = -\frac{g}{f}\frac{\partial \zeta}{\partial y} \tag{1}$$

$$v = \frac{g}{f}\frac{\partial \zeta}{\partial x} \tag{2}$$

with g the acceleration due to gravity, ζ the MDT, and $f = 2\Omega sin\phi$ the Coriolis parameter, where Ω is the angular speed of the Earth and ϕ is the latitude. Practically, the velocities are computed from central MDT differences. Thus, u and v are defined, centered between the two MDT grid points they are computed from. This two-point central difference computation of velocities minimizes smoothing. For practical reasons, the absolute velocity

$$w = \sqrt{u^2 + v^2} \tag{3}$$

is, however, defined on the MDT grid applying u and v north and east of the grid point, respectively.

2.2. Geostrophic Currents from Near-Surface Drifter Data

The drifter data applied in this study are the 6-hourly data set as provided by the Global Drifter Program (GDP, Lumpkin & Pazos, 2007). Only drogue-on drifters are applied (Lumpkin & Johnson, 2013). Available data until December 2014, made up of more than 10 million entries, are used. To estimate the time average surface geostrophic circulation, as can be drawn from the MDT maps, a number of corrections are necessary, applying external data wind (NCEP/NCAR reanalysis, Kalnay et al., 1996) and updated merged

sea level anomaly (SLA) provided by the Copernicus Marine Environment Monitoring Service (CMEMS). The methodology generally follows the description in Siegismund (2013), specifically subtracting wind slip of surface buoys, the filtering for inertial currents, and subtracting the time variable part of the geostrophic currents calculated from SLA, re-referenced to the period 2002–2013 and linearly interpolated to the drifter positions and time.

However, to secure complete independence of drifter data from any MDT used in this study, the estimation of Ekman currents does not use an MDT as reference. Instead, anomalies of the filtered drifter velocities within 5° × 5° boxes are calculated. The work of Rio and Hernandez (2003) and Ralph and Niiler (1999) is followed, but instead of the total Ekman current $\vec{U}_e$, the anomaly $\vec{U}'_e$ is estimated as

$$\vec{U}'_e = b\left(\frac{\vec{\tau}}{\sqrt{f|\tau|}}\right)' e^{i\Theta} \tag{4}$$

with $\tau = c_d * \rho * U_w * |U_w|$ the wind stress, where $c_d = 2.7 * 10^{-3} * |U_w|^{-1} + 1.42 * 10^{-4} + 7.64 * 10^{-5} * |U_w|$ and $|U_w|$ the wind speed. $'$ stands for the deviation from the temporal mean for the considered box. b and Θ are determined by least-squares (LS) fitting $\vec{U}'_e$ to the drifter velocity anomalies for each box. No LS fitting is performed for boxes containing not more than 1,000 data points.

All other boxes are checked for unrealistic estimates of b and Θ. Therefore, 1 m s^{-1} westerly wind is supposed and the Ekman current for the box and mean as well as standard deviation of both vector components of the Ekman current for the surrounding eight boxes are computed. If for at least one vector component the Ekman current of the considered box deviates from the mean of the surrounding boxes by more than 2.5 times the standard deviation, the LS fit is identified as outlier. The check for outliers is iterated for all boxes several times until no outliers remain.

For those boxes with too few drifter data points for the LS fitting or where the results of the fitting are detected as outliers, b and Θ are a function of the parameters in the surrounding boxes. b is obtained as weighted average. The weighting is set proportional to the reciprocal center-center distance between the boxes. To obtain Θ, the Ekman currents for westerly wind are summed but with the lengths of the vectors corrected to the same weighting as used to calculate b. Θ is then set as $\Theta = atan(v_e/u_e)$ with u_e (v_e) the zonal (meridional) component of the vector. For every data point, the Ekman currents are calculated and subtracted from the filtered drifter velocities to obtain estimates of temporal mean geostrophic currents at the positions of the filtered drifter velocities.

For the calculation of surface geostrophic velocities across sections as is discussed in section 4, all velocities from drifters crossing the section are taken into account. The velocity on the section is estimated as the average of the velocity vector before and after the crossing projected to the direction perpendicular to the section. To achieve a substantial averaging out of errors, from all crossing points, all possible 19 neighboring points are grouped. A weighted average of both velocity and position is computed for each group applying a reciprocal total velocity weighting (Maximenko, 2004), with the total velocity the sum of geostrophic, Ekman, and wind slip component.

Root mean square (RMS) differences of drifter- and MDT-derived geostrophic velocities as discussed in section 3 are based on evaluations for all drifter velocities in a specified region. The evaluation includes the comparison of the zonal and the meridional velocity component. For the geostrophic velocities derived from the MDT, the two components are defined on different grids. The zonal (meridional) component is defined central between two neighboring MDT grid points on the same longitude (latitude). For a specific drifter data point and component, the MDT-derived geostrophic velocity is linearly interpolated from the nearest three grid points for this component. The (MDT-drifter) difference in surface geostrophic velocity is determined as

$$\Delta w = \sqrt{(\Delta u)^2 + (\Delta v)^2} \tag{5}$$

with Δu (Δv) the difference in the zonal (meridional) velocity component. To obtain spatial mean RMS values not biased by the uneven distribution of the drifter data points, the squared velocity differences are

averaged over the boxes of a $1° \times 1°$ grid and then averaged over the region considered before the square root is applied.

2.3. Hydrodynamic Model

The hydrodynamic model applied is the MIT general circulation model (Marshall et al., 1997) covering the Arctic Ocean and the Atlantic Ocean north of 33°S in a horizontal resolution of 4 km. The model was set up with a bipolar curvilinear grid, with one pole located over North America and the other over Europe. In the vertical, the model setup uses 100 levels of varying depth, from 5 m in the upper ocean to 185 m in the deep ocean. Bottom topography is derived from the ETOPO database in 2′ resolution. The model starts from the year 2002 conditions from another model that has a similar setup with lower resolution of approximately 8 km and itself starts in 1948 from the annual mean temperature and salinity from the World Ocean Atlas 2005 (Boyer et al., 2005). The model simulation spans the period from 2003 to 2009.

The model simulation is forced at the surface by fluxes of momentum, heat, and freshwater computed using bulk formulae and the 6-hourly atmospheric state from the 1989 to 2009 ECMWF ERA-Interim reanalysis (Dee, 2011). At the open southern boundary, the simulations are forced by the output of a 1° resolution global solution of the MITgcm forced by the NCEP data set. A barotropic net inflow of 0.9 Sv (1 Sv $=10^6 m^3 s^{-1}$) into the Arctic is prescribed at Bering Strait, the model's northern open boundary, which balances a corresponding outflow through the southern boundary at 33°S. A dynamic thermodynamic sea ice model solves for sea ice parameters. See Biri et al. (2016) for details.

For the purpose of this study, the modeled sea level is saved on a $10' \times 10'$ grid applying bilinear interpolation. For regions outside the model grid, a Laplacian smoother (see Appendix A) is applied to obtain a global MDT. The Laplacian smoother solves the Laplacian equation $\Delta\zeta = 0$, with the MDT values at the margin of the model grid as boundary condition. Different spatial resolutions are realized by successive SH analysis and synthesis steps. Geostrophic currents are obtained with the same method as applied for the geodetic MDTs.

3. Global MDT

Geodetic MDTs are derived from the difference of MSS and geoid height. A common way to solve the spectral inconsistency between the MSS and the geoid is to fill the land areas of the MSS with geoid information and then low-pass filter the globalized MSS by performing an SH analysis and cutting off short scales above maximum d/o of the geoid.

However, two sources of inconsistency remain after globalizing the MSS that cause unphysical MDT signal when cutting off small-scale information in the MSS:

1. a step along the coast line with its height depending on the local amplitude of the MDT and
2. the inconsistency between the geoid filled in over land and that contained in the MSS over the ocean.

It is suggested here to globalize the MDT smoothly applying Laplace's equation to obtain land values. The coastal MDT values are used as boundary conditions. The mathematically extended MDT land values added to a high-resolution geoid model provide a globalization of the MSS that strongly reduces the inconsistency.

3.1. Idealized Example

An idealized example is provided now to illustrate the impact of common MSS land-filling approaches compared with the suggested new methodology onto the quality of the MDT (see workflow in Figure 2). A real data comparison of MDTs obtained from different approaches including the one proposed here is provided in section 3.2 below.

Figure 3a displays the North Atlantic MDT obtained from the MIT hydrodynamic model explained in section 2.3. The MDT has been sampled on a $10' \times 10'$ grid and has thus a unique spectral representation up to d/o 1,080. For our example, we consider this model ζ as a perfect, error-free MDT of the North Atlantic. The signal beyond d/o 1,080 is neglected. This MDT is used to assess the quality of both MDTs derived from conventional MSS globalization approaches and the new one proposed here. As a geoid model N, we apply the GECO model synthesized to maximum d/o 1,080. We suppose also this model to be error free. The perfect ocean values for the MSS h are then defined as the sum of ζ and N.

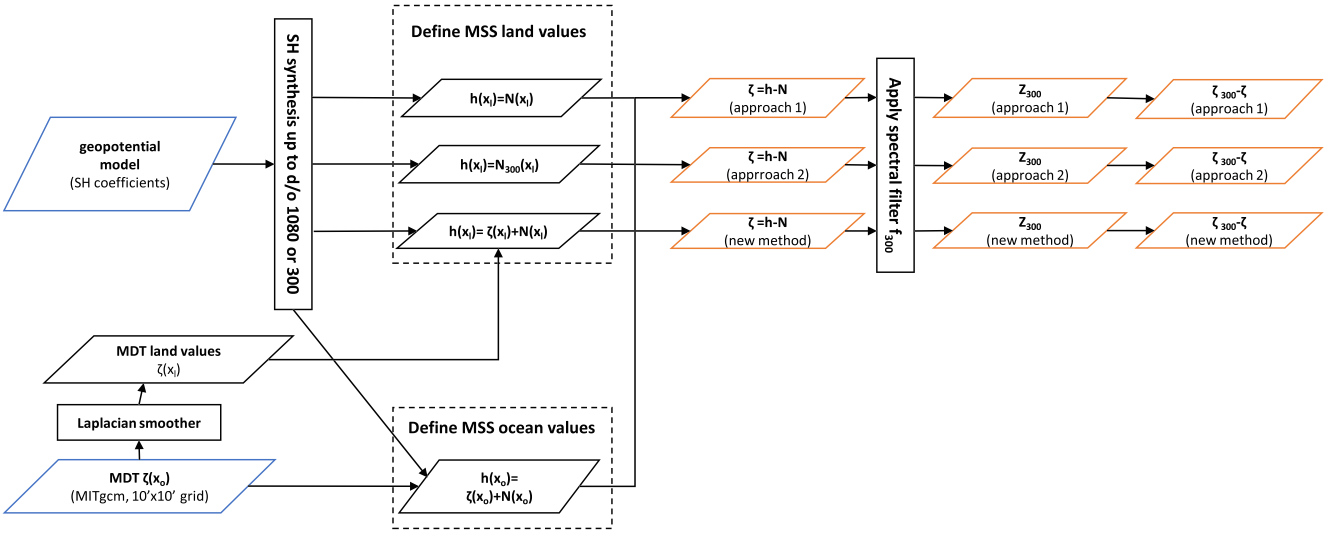

Figure 2. Workflow for the computation of MDTs in the idealized example. The blue and orange bordered rhomboids show the input data and the output MDTs mapped in Figure 3, respectively. The spatial arrangement of the orange bordered rhomboids corresponds to the arrangement of the panels of Figure 3.

In practice, MSS models are available in high resolution and we apply for our example the just defined perfect MSS model. For the geoid height, we might want to work for example with a satellite-only geopotential model, which nowadays is resolved up to maximum d/o 300. To consider this case, we apply again our perfect geoid model N, this time cut at maximum d/o 300 (called N_{300} hereafter). This means that in our idealized case, the only error of the geoid model is the omission error $N - N_{300}$ for the missing signal beyond d/o 300.

The MSS has now to be globalized and spectrally cut off to maximum d/o 300 according to the spectral method described by Bingham et al. (2008). For globalizing the MSS, two approaches are common:

1. the MSS is filled with a high-resolution geoid model, which in case of a perfect geoid model means MDT = 0 over land, and
2. the MSS is filled with the same (low-resolution) geoid model as that applied later to obtain the MDT.

To illustrate the first approach, we apply

$$h(x_l) = N(x_l) \tag{6}$$

for an arbitrary land point x_l; thus, our perfect geoid model N provides the MSS land values. In our example, all grid points outside the modeled North Atlantic are defined as land points, but this constraint does not limit the conclusions. After cutting off the MSS at d/o 300 and subtraction of N_{300}, the resulting MDT ζ_{300} is displayed in Figure 3b. Due to the linearity of the spectral filter f_n for an arbitrary cut-off d/o $n \in \mathbb{N}$, the sequence of subtraction and spectral filtering can be swapped, so

$$\zeta_{300} = f_{300}(h) - f_{300}(N) = f_{300}(h - N) = f_{300}(\zeta) \tag{7}$$

Since N is known, we also know the MDT ($=h - N$) before the spectral filtering. Those MDTs, which are differences from a globalized MSS and a geoid model, are called global MDTs here. The global MDT for approach 1 is the one displayed in Figure 3a. Since $h = N$ over land, the global MDT is zero here.

To illustrate the second approach, we apply

$$h(x_l) = N_{300}(x_l) \tag{8}$$

for an arbitrary land point x_l.The global MDT for this approach is displayed in Figure 3d. The values over land are equal to the negative geoid signal between d/o 301 and 1,080, reflecting the different spectral resolution of our perfect geoid model and the MSS land values. The final MDT after cutting off the MSS at d/o 300 and subtraction of N_{300} is shown in Figure 3e.

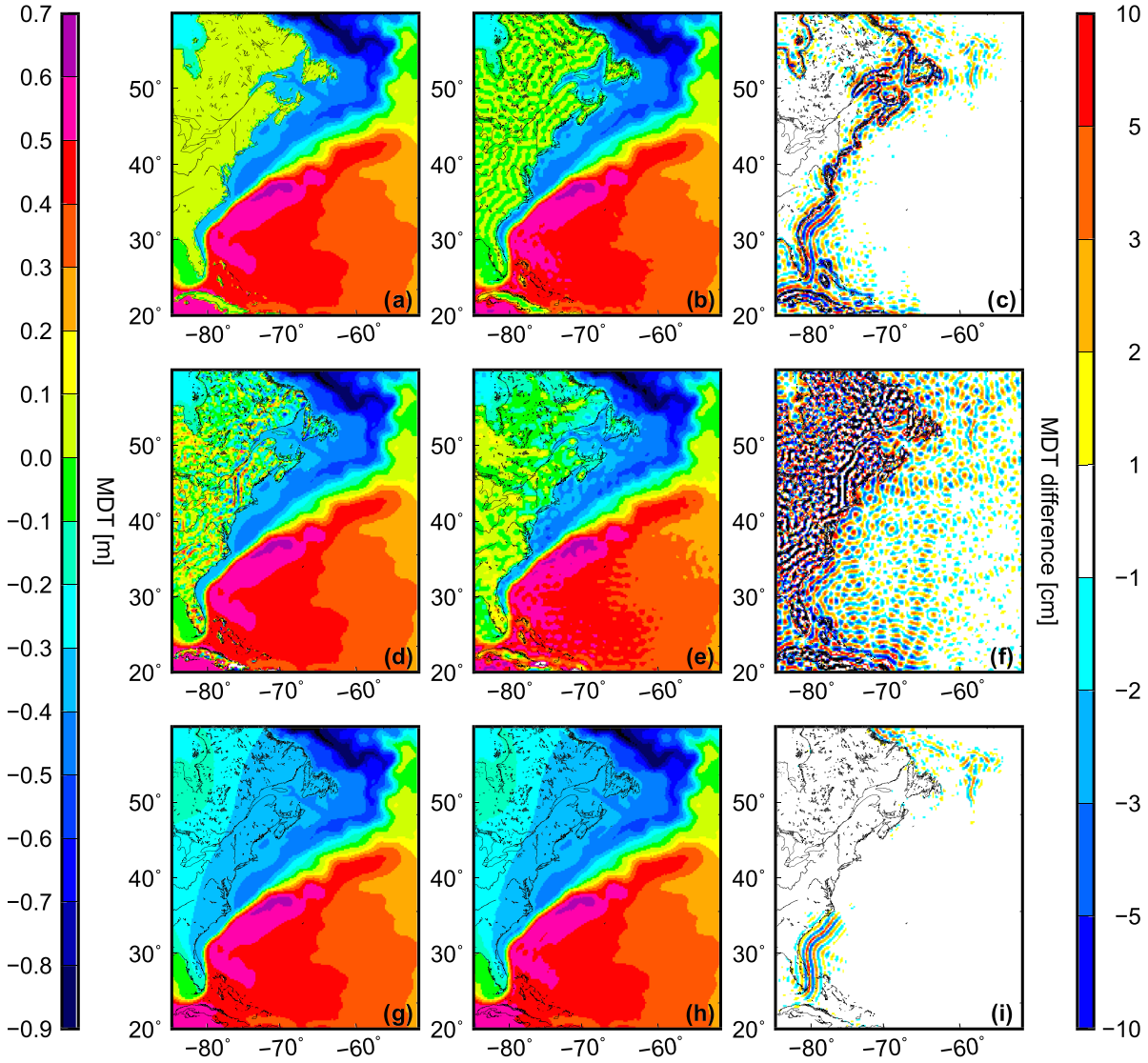

Figure 3. MDTs (m) in an idealized example resulting from different approaches for MSS land value determination. The nine panels shown correspond to the nine orange bordered rhomboids of the workflow displayed in Figure 2. (a, d, g) The "error-free" MDTs, only different in their land values, which result from different approaches for globalizing the MSS. (b, e, h) Spectrally filtered MDTs with a maximum d/o of 300. (c, f, i) Differences of "error free" and spectrally filtered MDTs. (a, b, c) correspond to the first approach, (d, e, f) correspond to the second approach, and (g, h, i) display results from the proposed new approach. See text for details.

The difference of the MDTs derived from the two approaches and the high-resolution perfect MDTs is shown in Figures 3c and 3f, respectively. Besides the stripes following the Gulf Stream and the Labrador Current, a short-scale wave pattern is seen along the coast line for both cases and also away from the coasts in the second case. The amplitudes reach 10 cm over the ocean and, specifically for the second case, larger values over land.

The stripes following the strong currents are an effect of non-sufficient resolution to resolve the physical phenomenon and reduction of errors there will need a higher resolution geoid model than d/o 300. The wavy structure, however, is an effect of the land-ocean MSS (and MDT) step and the mentioned land-ocean geoid inconsistencies.

The new methodology for globalizing the MSS is able to strongly mitigate this wavy structure. In this approach, rather than filling the MSS barely with geoid values, a land MDT is added to mitigate the $(h - N)$ step along the coast line. The MDT land values $\zeta(x_l)$ are defined as a smooth continuation of the coastal

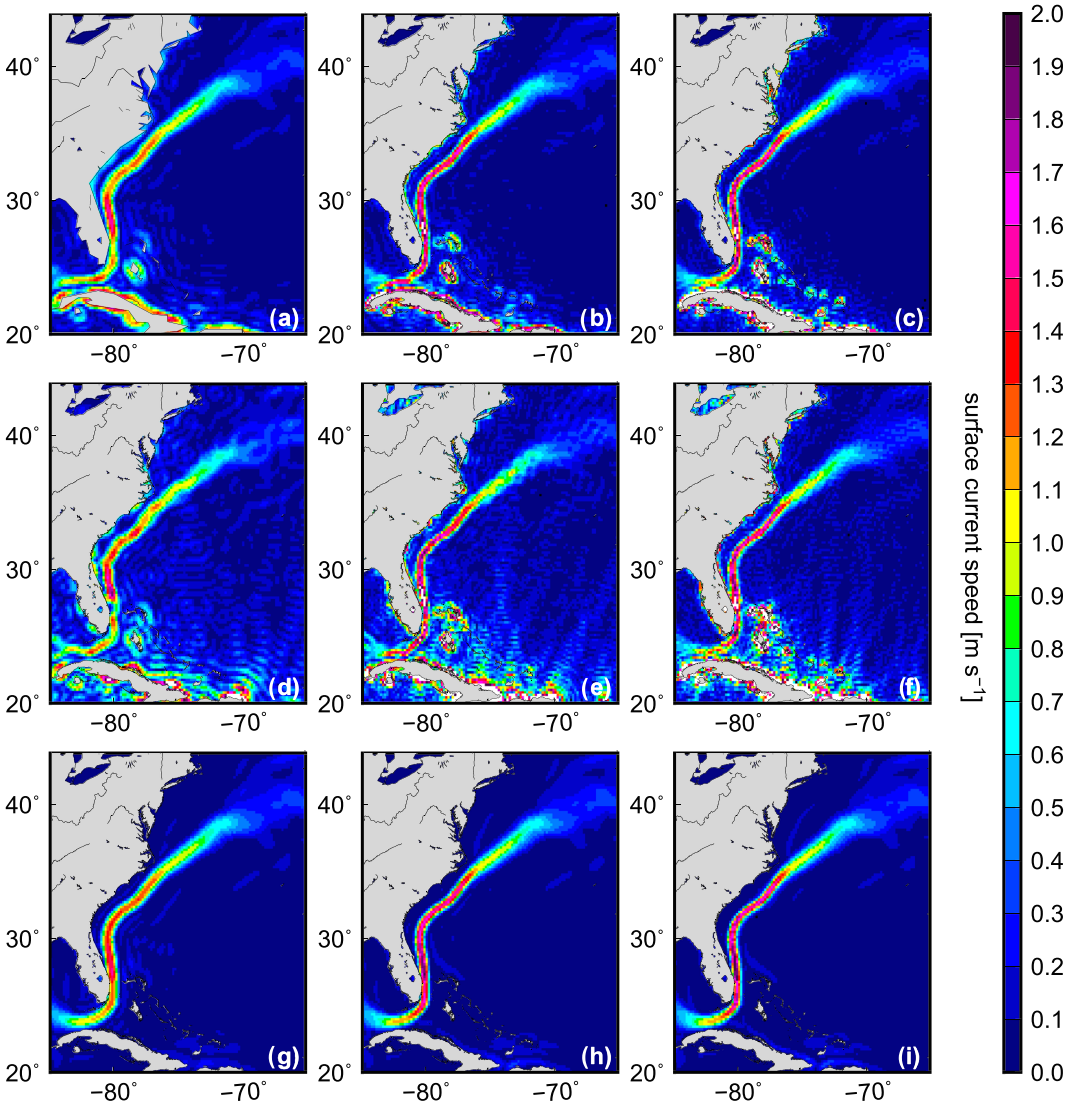

Figure 4. Absolute surface geostrophic currents (m s^{-1}) obtained from an idealized example. (a, b, c) First approach, (d, e, f) second approach, and (g, h, i) new approach. Maximum d/o of corresponding MDTs are (a, d, g) 300, (b, e, h) 480, and (c, f, i) 720. See text for details.

MDT values $\zeta_c = \zeta(x_c)$ for a coastal point X_c. This is realized by solving Laplace's equation over land with ζ_c as boundary condition. This corresponds to solving the two-dimensional heat equation without sources. How this is realized in our case is explained in Appendix A.

For the coastal MDT values $\zeta(x_c)$, for an arbitrary coastal point x_c, we take in our example the difference $h(x_c) - N(x_c)$ of our perfect geoid and ocean MSS models, which is the perfect MDT by definition. In practical applications, of course, the MDT is the unknown. The conventional MSS globalization, however, implies MDT = 0 over land. MDT estimates, which substantially reduce the land-ocean step caused by this implication, can easily be made by applying available MDTs from geodetic observations or hydrodynamic models. A real-data test for the different approaches illustrated in this example is provided in section 3.2.

The resulting globalized MDT is shown in Figure 3g and the spectrally filtered MDT in Figure 3h. As expected, the spectral filter produces substantially weaker wavy structures (see Figure 3i) than in the other two approaches. Even more pronounced effects are observed for the absolute geostrophic surface currents w (Equations 1–3). Figure 4 shows w for the three approaches for different cut-offs n of the MDT. The left column shows the results for $n = 300$ and thus corresponds to the MDTs shown in Figure 3. The middle (right)

column corresponds to $n = 480$ ($n = 720$). As expected, the wavy structure is less pronounced and the effect of the proposed methodology is weaker when the cut-off is defined at a higher maximum d/o. However, almost no obviously unphysical signals are seen with the proposed new approach. The remaining stripes adjacent and parallel to the Gulf Stream are probably an unavoidable effect from cutting off the small scales of the currents. This effect weakens for higher maximum d/o.

3.2. Methodology

From the example above, we conclude that the quality of a geodetic MDT depends not only on the accuracy of the applied MSS and geoid models, but also on the definition of MSS (or MDT) land values. Three different approaches for MSS land value definition have been tested. For each approach, through the idealization, the final MDT resulted from spectrally filtering a high-resolution global MDT with identical ocean but different land values among the approaches. The proposed new approach with a smooth land definition and vanishing ocean-land step in its high-resolution MDT has been the best with respect to minimization of unwanted Gibbs effect in the spectrally filtered MDTs.

The idea behind the proposed approach is that a geodetic MDT should always be sought as a spectrally truncated high-resolution MDT ζ_{hf} with a smooth pattern over land and a continuous ocean-land transition. For ζ_{hf}, we thus define the land values by solving Laplace's equation

$$\Delta\zeta_{hf}(x_l) = 0 \tag{9}$$

for all land points x_l with the set ζ_c of all coastal values $\zeta_{hf}(x_c)$ as boundary condition. As result, for an arbitrary land point x_l, we obtain

$$\zeta_{hf}(x_l) = g(\zeta_c, x_l) \tag{10}$$

with g the function determined by Laplace's equation.

As a geodetic MDT, ζ_{hf} is thought as the difference of high-resolution MSS and geoid models, for example,

$$\zeta_{hf} = h_{hf} - N_{hf} \tag{11}$$

The spectrally filtered geodetic MDT with maximum d/o n is then

$$\zeta_n = f_n(\zeta_{hf}) = f_n(h_{hf} - N_{hf}) = f_n(h_{hf}) - f_n(N_{hf}) = h_n - N_n \tag{12}$$

where h_{hf} is defined as

$$h_{hf}(x) = \begin{cases} h_o(x) & \text{if } x \text{ is an ocean point} \\ N_{hf}(x) + \zeta_l(x) = N_{hf}(x) + g(\zeta_c, x)) & \text{if } x \text{ is a land point} \end{cases} \tag{13}$$

with h_o the ocean-defined MSS model.

In practical applications, h_o and N_n are estimated from an available MSS model and the geoid model selected over the ocean. n might be the maximum d/o of the selected geoid model, or the model is provided with a higher maximum d/o but is cut at this resolution, for example, to reduce the commission error.

The definition of the MSS land values needs a high-resolution coastal MDT ζ_c to obtain ζ_l and a high-resolution geoid model to estimate N_{hf}. To compute ζ_c, we subtract a geoid model from the coastal MSS. The same geoid model is added to the globalized MDT to obtain MSS land values. In general, a hydrodynamic model could also be applied to obtain a high-resolution ζ_c. But any inconsistency of data used left and right of the coast line can cause a step in $h - N$ and is avoided here.

The globalized MSS can in general be provided in any resolution m at or above maximum d/o n of the desired MDT and is then spectrally cut as described in Equation 12. The decision for m will depend on two issues:

1. since any low-pass filtering is prone to Gibbs-like effects, the globalization should be performed as close as possible to the resolution that the MSS is originally provided with, and
2. geoid information over land has to be available, consistent with the chosen resolution m.

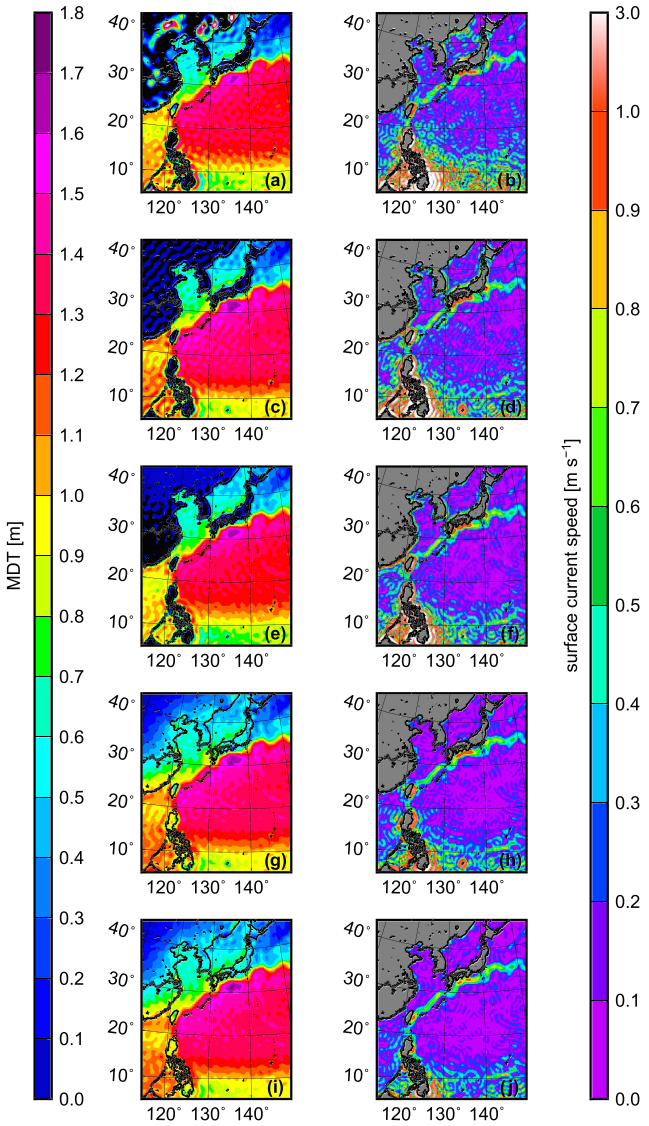

Figure 5. MDT (left, in m) and geostrophic currents (right, in m s^{-1}) as obtained from the five different approaches for land filling the MSS. Each row refers to one approach in the same order as in the enumerated list in the text.

Geoid models are nowadays available up to d/o 2,160, and it is recommended to use this resolution for the land filling of the MSS. However, no highly accurate routines have been available for this study to perform SH analysis and synthesis for high-resolution global fields. Maximum d/o will be 1,080 here, which is, however, sufficient to show the impact of the approach to the resulting MDT. It is worth noting at this point that the coastal MDT determined to globalize the MSS is not seen as physical signal in the resulting MDT in the end. It is just a means to compute the "land MDT" added to the geoid. It is thus not inconsistent to apply the suggested MSS globalization applying a high-resolution combined geoid model and use a satellite-only geoid model to compute the MDT at the end.

The suggested full procedure to compute a global MDT is as follows.

1. A gridded MSS is provided in the spectral resolution of the geoid model applied to compute the MSS land values. We apply DTU15, which is provided on a $1' \times 1'$ global grid and apply a spectral analysis/synthesis step to reduce the resolution to maximum d/o 1,080 computed on a $10' \times 10'$ grid.
2. The geoid chosen for the globalization/correction of the MSS is subtracted to obtain a high-resolution MDT ζ_{hf}. We use here different geoid models (see below).
3. The land-sea mask necessary to identify the grid points that need a filling is provided by the GOCE User Toolbox (GUT), which is also applied for all analysis/synthesis and spatial filtering issues. For outlier detection, the geostrophic surface currents based on the ocean points of ζ_{hf} are computed. For both current vector components, if velocity exceeds 3 m s^{-1}, the involved grid points are set to land. This is done to minimize influence of potentially large local MSS errors onto the MDT at some locations near the coast.
4. Based on the coastal values of ζ_{hf}, the MDT land values $\zeta(x_l)$ are computed, applying the Laplacian equation.
5. $\zeta(x_l)$ is added to the geoid and used as land values for the MSS.
6. The MSS is successively analyzed/synthesized to the spectral resolution n and the desired grid of the resulting MDT.
7. The geoid is computed for maximum d/o n on the same grid as the MSS.
8. The geoid height is subtracted from the MSS to obtain the global MDT.
9. MDT land values are set to NaN.
10. A spatial filter is applied, if necessary.

3.3. Impact of MSS Correction Onto MDT Errors

The suggested methodology creating a global MSS is now tested in a practical example. We want to obtain an MDT from DTU15 and the TIM_R6 geoid model. Four approaches to obtain a global MSS are tested.

1. DTU15 is already a global model and is taken as is.
2. TIM_R6 is used to fill in over land. This is the same model that is subtracted from the MSS to obtain the MDT.
3. GECO up to maximum d/o 1,080 is filled in over land.
4. Coastal MDT (ζ_c) is computed by subtracting the GECO geoid model truncated at maximum d/o 1,080 from the MSS. MSS land values are computed following Equation 13, applying TIM_R6 for geoid land values $N_{hf}(x_l)$. This approach minimizes the ocean-land step along the coast lines, but the geoid inconsistency over land remains.
5. Coastal MDT ζ_c is computed as in 4, but the GECO geoid model up to d/o 1,080 is also applied for land values $N_{hf}(x_l)$ in Equation 8. This approach is expectedly the best of the five approaches.

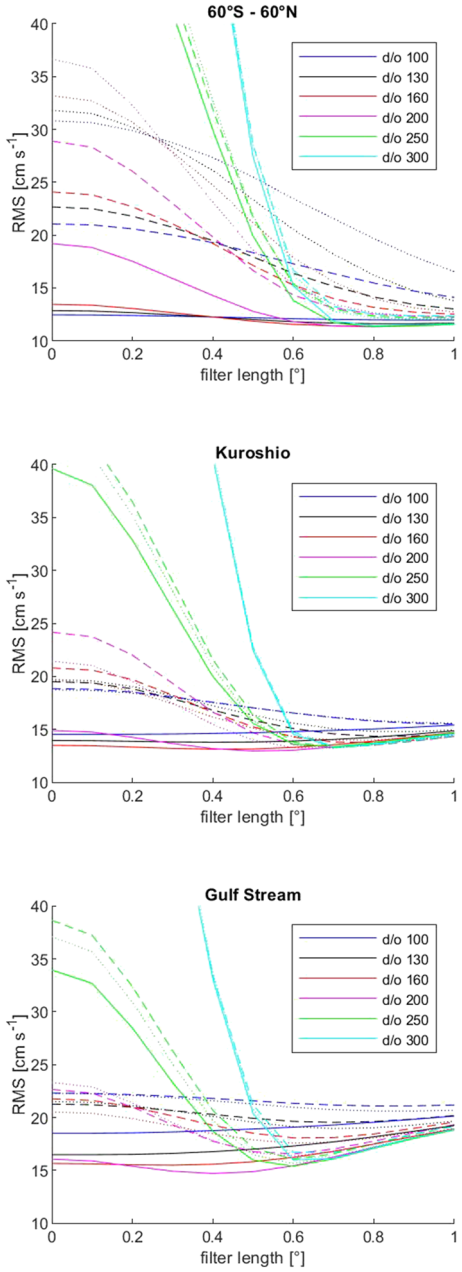

Figure 6. RMS differences (cm s^{-1}) of geostrophic surface currents as obtained from geodetic MDTs and corrected near-surface drifter velocities. The MDTs are based on TIM_R6 as geoid models and are computed applying approaches 1, 2, and 4 displayed as dotted, dashed, and solid lines, respectively. The three panels show results for (top) the latitudinal band from 60°S to 60°S, (middle) the Gulf Stream region (20°–40°N, 85°–60°W), and (bottom) the Kuroshio (20°–40°N, 120°–155°E). For each model and region, MDTs with maximum d/o as listed in the inset and applying a truncated Gaussian filter with filter lengths [0.0°, 0.1°, … 1.0°] are tested.

The result of the five approaches is displayed in Figure 5 for the Kuroshio. The first three approaches (Figures 5a to 5f), which all include a step in global MDT along the coast line, produce false strong MDT gradients near the coast in some regions and thus unrealistic high surface geostrophic currents. Interestingly, in these approaches, the small-scale wavy structure far away from the coast is also more pronounced than in the remaining two methods. This shows that the way the MSS is globalized is not only important for coastal processes but has also significant offshore effects. If Laplacian smoothing is applied to add a smooth MDT signal to the land MSS, it remains the choice for the geoid model added to the MDT signal to obtain the MSS over land. If, in our test case, the low-resolution TIM_R6 model is applied (Figures 5g and 5h), still unrealistic high currents result at some individual locations near the coast line, which are not seen when the high-resolution GECO model is applied (Figures 5i and 5j). In summary, spectral inconsistency of the MSS and the geoid model applied for the land fill in causes regional errors. But the land-sea step in MDT is clearly the more important issue when globalizing the MSS with impact on the global ocean. We will thus concentrate in the following on approaches 1 and 2, which both include the land-sea step and have been used in the past to compute geodetic MDTs, and approach 5, which we propose here as the best strategy for globalizing the MSS.

For a specific, regional or global application, the choice of the MDT will depend on specific criteria or metrics. As a useful example, we apply here the comparison to near-surface drifter data to find the best MDT for two regions (around the Gulf Stream and the Kuroshio) and the latitudinal band between 60°S and 60°N. Applying DTU15 as MSS and TIM_R6 as geoid model as before, two parameters of the MDT computation recipe as listed in section 3 are varied to find that MDT which fits best the drifter data in the region considered:

1. the maximum d/o of the MDT and
2. the length scale of the truncated Gaussian kernel applied as spatial filter

For all regions, the cut-off both at maximum d/o 250 and 300 produces rather large RMS values below filter length of 0.6° for all three approaches (Figure 6) and should not be used. For lower maximum d/o, the MDT obtained with approach 4 fits better to the drifter data for all filter lengths and all regions. Specifically for short filter scales and high d/o needed to resolve small-scale currents, the RMS for approach 4 is much lower than for the other two approaches. Quality differences of MDTs from approaches 1 and 2 are not that clear. While globally (60°S–60°N) approach 2 is closer to the drifter data, for the Gulf Stream and the Kuroshio region, RMS values for both methods are rather close.

For the Gulf Stream, the MDT model following approach 4 with maximum d/o 200 and a filter scale of 0.4° fits with an RMS difference of 14.7 cm s^{-1} best to the drifter data. The best model applying a different MSS globalization approach is an MDT with maximum d/o 250, 0.6° filter scale, and following approach 2. The RMS difference here is 16.1 cm s^{-1}. Geostrophic surface currents based on these two MDT models are displayed in the top panels of Figure 7. It is clearly seen that though MSS and geoid include small-scale information up to d/o 250, due to the stronger spatial filtering necessary when approach 2 is applied, maximum speed in the core of the Gulf Stream is much weaker than for approach 4. Similar results are found for the Kuroshio (bottom panels of Figure 7), though with somewhat smaller differences in velocities from different approaches. The cut-off maximum d/o is the same as for the Gulf Stream for each of the approaches while the filter scales are 0.1° longer.

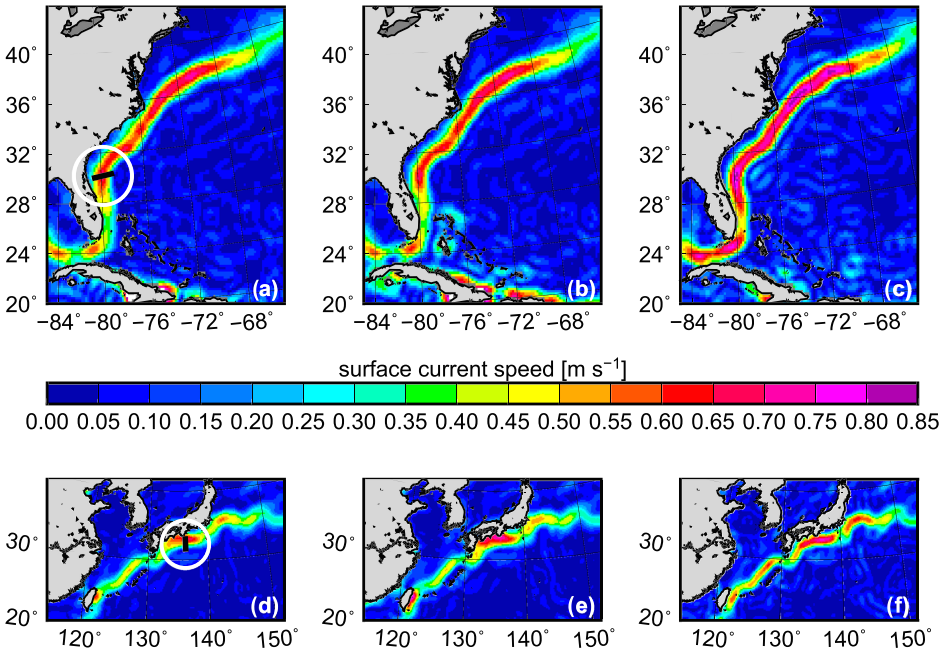

Figure 7. Geostrophic surface velocities (m s^{-1}) from optimized MDT models applying TIM_R6 as geoid model. Optimization is performed for (a, b, c) the Gulf Stream region (20°–40°N, 85°–60°W) and (d, e, f) the Kuroshio (20°–40°N, 120°–155°E) by minimizing the RMS difference to corrected near-surface drifter data with respect to different maximum d/o and spatial filter length applied to the MDT. The optimization is done for each of the applied MSS globalization approaches. For (a, d) approach 1 and (b, e) approach 2, optimal maximum d/o is 250 for both regions, while filter length is 0.6° (0.7°) for the Gulf Stream (Kuroshio). For (c, f) approach 4, optimal maximum d/o is 200 for both regions and filter length is 0.4° (0.5°) for the Gulf Stream (Kuroshio). Sections crossing (a) the Gulf Stream and (d) the Kuroshio are plotted as thick black lines within a white circle. On these sections, direct comparisons of drifter and MDT-derived geostrophic (near-)surface currents are performed (see Figures 9 and 10).

4. Choice of Maximum d/o

For the satellite-only geoid model TIM_R6 we applied in the last section, we have already seen that it is not recommended to use this model up to its full resolution of d/o 300. Application of other satellite-only geoid models has revealed similar results (Siegismund, 2013). This might be inevitable due to large commission errors in high d/o SH coefficients, though anisotropic filtering might relax this issue (Bingham, 2010; Cunderlik et al., 2013). With the usual way of globalizing the MSS, Gibbs effects are inevitable due to both inconsistencies between land and ocean geoid models and the land-ocean step. These effects grow with reducing the spatial resolution of the MDT. Thus, to minimize these effects, a high maximum d/o is needed, regardless if oceanographic signal is included in the small scales. As an example, the XGM geoid model is applied to compute (unfiltered) MDTs for maximum d/o 300 to 720 for approaches 1 and 4. Figure 8 displays the RMS differences of geostrophic surface currents from these MDTs and the corrected near-surface drifter velocities.

It has to be stated that when considering global performance already, for maximum d/o 300, the bulk of the MDT signal is resolved since most of the global ocean is covered by large-scale gyres rather than small-scale currents. Thus, omitted MDT signal is not a dominant source of error. For approach 4, RMS differences are increasing with maximum d/o because of increasing noise in SH coefficients, while for approach 1, due to Gibbs effects, the RMS values are much higher and increase with decreasing maximum d/o.

With the Gibbs effects strongly reduced in approach 4, we mainly see the remaining noise in both the geoid model and the MSS and increasing with d/o. Though this noise is an intrinsic part of available MSS and geoid models, sophisticated anisotropic filtering might reduce the issue. However, the small-scale signal content of the MDT is generally limited by the observation strategy for both the MSS and the geoid. Thus, beyond a specific scale, no signal will be detectable in the resulting MDT. With generally growing commission error

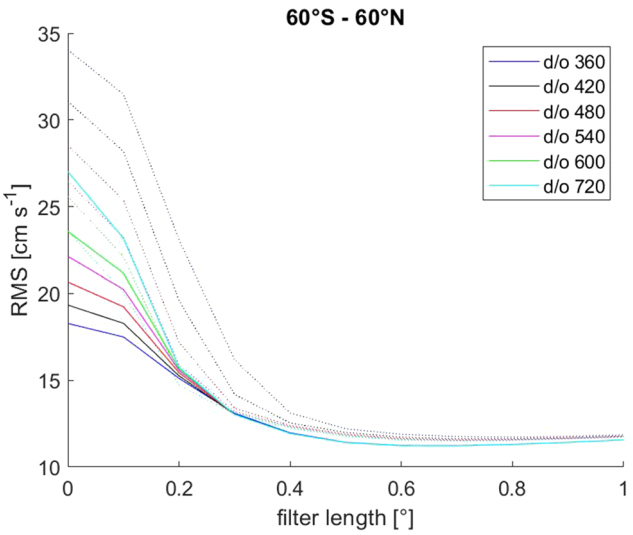

Figure 8. RMS differences (cm s^{-1}) of geostrophic surface currents as obtained from geodetic MDTs and corrected near-surface drifter velocities for the latitudinal band between 60°S–60°N. The MDTs include XGM as geoid model and are computed from approaches 1 and 4 displayed as dotted and solid lines, respectively. For both approaches, MDTs with maximum d/o as listed in the caption and applying a truncated Gaussian filter with filter lengths [0.0°, 0.1°, … 1.0°] are tested.

with higher d/o, it might be advisable to cut the MDT beyond this scale to minimize noise without losing signal.

Therefore, we address here the question up to which maximum d/o a signal is detectable in surface geostrophic currents from geodetic MDTs. The focus is set on the two strongest western boundary currents, the Gulf Stream and the Kuroshio. The short across-current scale needs small-scale information in the MDT to fully resolve the strong gradient in MDT, and the strength of the currents reduces the influence of the commission error as much as possible. For both the Gulf Stream and the Kuroshio, one section is selected (see Figures 7a and 7d). The selection is based on the high maximum velocity of the current at this position and the number of available drifter data, respectively.

We compute MDT models applying all six combined geoid models listed in Table 1. For the MDTs that result from subtracting EGM2008, Eigen-6C4, GECO, or SGG-UGM-1 from DTU15, the same geoid model is also used to obtain land geoid values for DTU15, while for GOCO05c and XGM, the GECO model is applied. Spectral resolution from maximum d/o 100 to d/o 1,080 is tested.

For the Gulf Stream, the MDT obtained from the hydrodynamic model is applied for comparison. For this issue, the model results are interpolated to a $10' \times 10'$ grid, the same as that used for the geodetic MDTs, and the Laplacian smoother is used to fill the grid points outside of the North Atlantic. Then, the globalized North Atlantic model is analyzed/synthesized to obtain MDTs on the desired maximum d/o.

Currents over a section could be characterized either by absolute speed or the velocity component perpendicular to the section. Errors in the MDT will systematically increase absolute speed assuming independence of the gradients observed in the MDT and in the error. To prevent potential bias in geostrophic velocities obtained from the geodetic MDTs, we consider therefore only the speed perpendicular to the section with random fluctuations caused by errors in the MDT. The accurate orientation of the sections is determined by minimizing along-section speed according to the drifter data.

For all MDT models and both sections up to d/o 420, maximum speed increases with increasing resolution (Figures 9 and 10). For this resolution, maximum velocities have considerable spread between the different MDT models. For the Gulf Stream (Figure 9), they reach between approximately 75% (Eigen-6c4) and 90% (GECO) of maximum velocity observed in the drifter data. For the Kuroshio (Figure 10), the geodetic MDTs are very close to the drifter data with the smallest maximum velocities for GOCO05c and Eigen-6c4 reaching around 93% of maximum drifter velocity. Beyond d/o 420, the development is heterogeneous for both currents, but no model shows substantial increase in maximum velocity. The spatial pattern of the current generally follows quite closely that observed by the drifter data for the Gulf Stream. Only the MDT based on the Eigen-6C4 geoid shows higher currents than all other models 50–100 km offshore from the maximum velocity axis. For the Kuroshio, the geostrophic currents from the geodetic MDTs do not follow the velocities observed by the drifters so closely. Different from the bell-shaped Gulf Stream, the profile of the Kuroshio offshore the maximum includes short-scale information. The best agreement with the drifter data in vicinity of the maximum is found for d/o 420. This corresponds to a spatial scale of 48 km, which is too wide to resolve the profile. For higher resolution, however, unphysical signals evolve, as the minimum around 30 km and a peak of strong velocity close to the point of maximum velocity as seen by the drifter data. The structure of the current for resolutions beyond maximum d/o 720, specifically for maximum d/o 1,080, is well off the pattern observed by the drifters. For the Gulf Stream, the maximum velocity of the MIT model increases strongly until d/o 480 and reaches maximum around d/o 720 close to maximum velocity of the drifter data though slightly shifted off coast.

To get a clearer view on the development of the MDT-derived geostrophic surface currents beyond d/o 420, we map the absolute velocities from all four high-resolution geoid models for both the Gulf Stream (Figure 11) and the Kuroshio (Figure 12) for maximum d/o 420, maximum d/o 1,080, and the difference

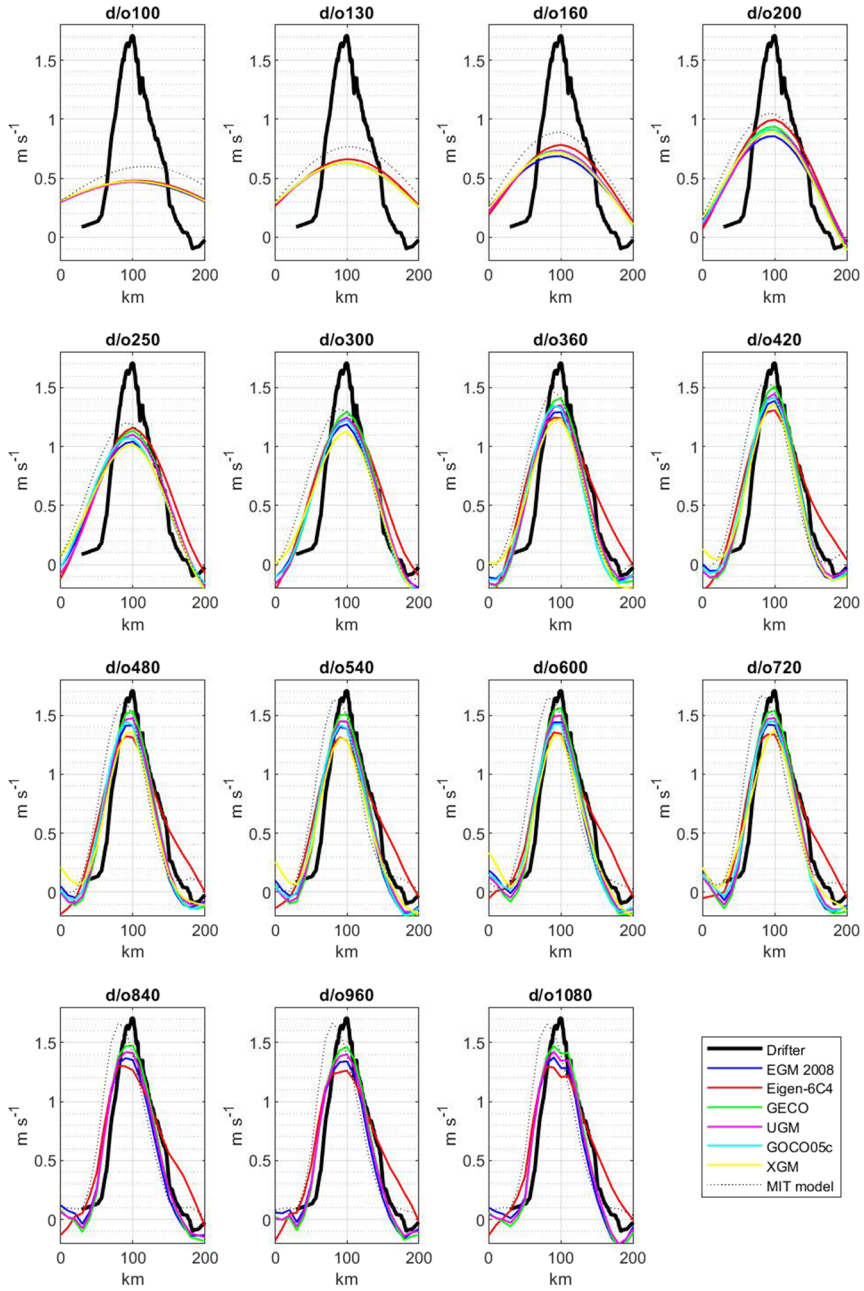

Figure 9. Geostrophic surface velocity (m s^{-1}) over a section across the Gulf Stream (see Figure 7a) with the distance over the section, measured from the coast line and thus increasing from west to east, provided in kilometer. Only the component perpendicular to the section is considered. As listed in the inset, geostrophic surface currents from drifter data and from geodetic and hydrodynamic MDTs are shown. The MDTs are SH analyzed/synthesized for a set of selected resolutions from maximum d/o 100 to 1,080, each resolution shown in a separate panel.

(d/o 1,080 minus d/o 420). From the comparison of the currents itself, for both the Gulf Stream and the Kuroshio, the differences in velocities are hardly detectable. From the mapping of the difference, we see for the North Atlantic a structure that seems to follow the Gulf Stream. However, analyzing the geoid height, we see strong gradients east of the North American east coast and differences in the currents comparing different models beyond d/o 420 seem largely influenced by this effect in the geoid. Much stronger geoid gradients are found in the Northwest Pacific along the margin of the Philippine Plate. Partly, this margin follows closely the path of the Kuroshio, and it is not clear whether the differences seen in the currents

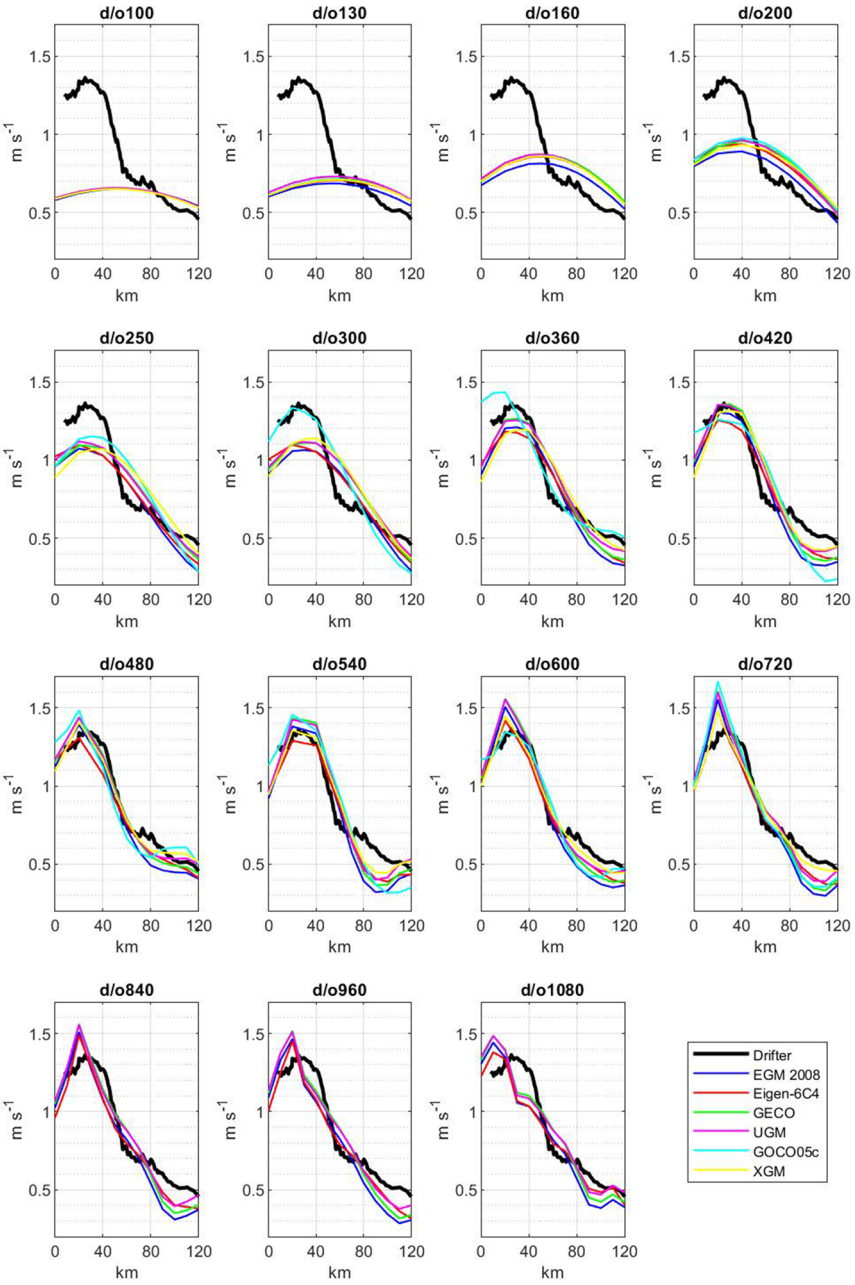

Figure 10. Same as Figure 7, but for a section over the Kuroshio (see Figure 7d), with the distance on the abscissa provided relative to the coast line and thus increasing from north to south.

for different spectral resolution are signals in MDT or resolution-dependent spatial patterns caused by the inconsistency between geoid and MSS in the presence of a strong geoid gradient.

5. Conclusions

The computation of the geodetic MDTs as the difference of the MSS and the geoid needs spectral consistency of the two fields. Since the geoid is usually derived from Stokes coefficients describing the geopotential field, their natural representation is a linear combination of SH functions with cut-off at a specific maximum d/o. To obtain the same representation for the MSS, a globalization is needed. This is usually done by filling in a geoid model over land. This approach, however, causes unphysical wavy structures in the MDT caused by the Gibbs phenomenon from the ocean-land discontinuity in the MSS that reflects the amplitude in coastal MDT and from spectral inconsistency of the geoid filled in on land and MSS-MDT over the ocean. The new

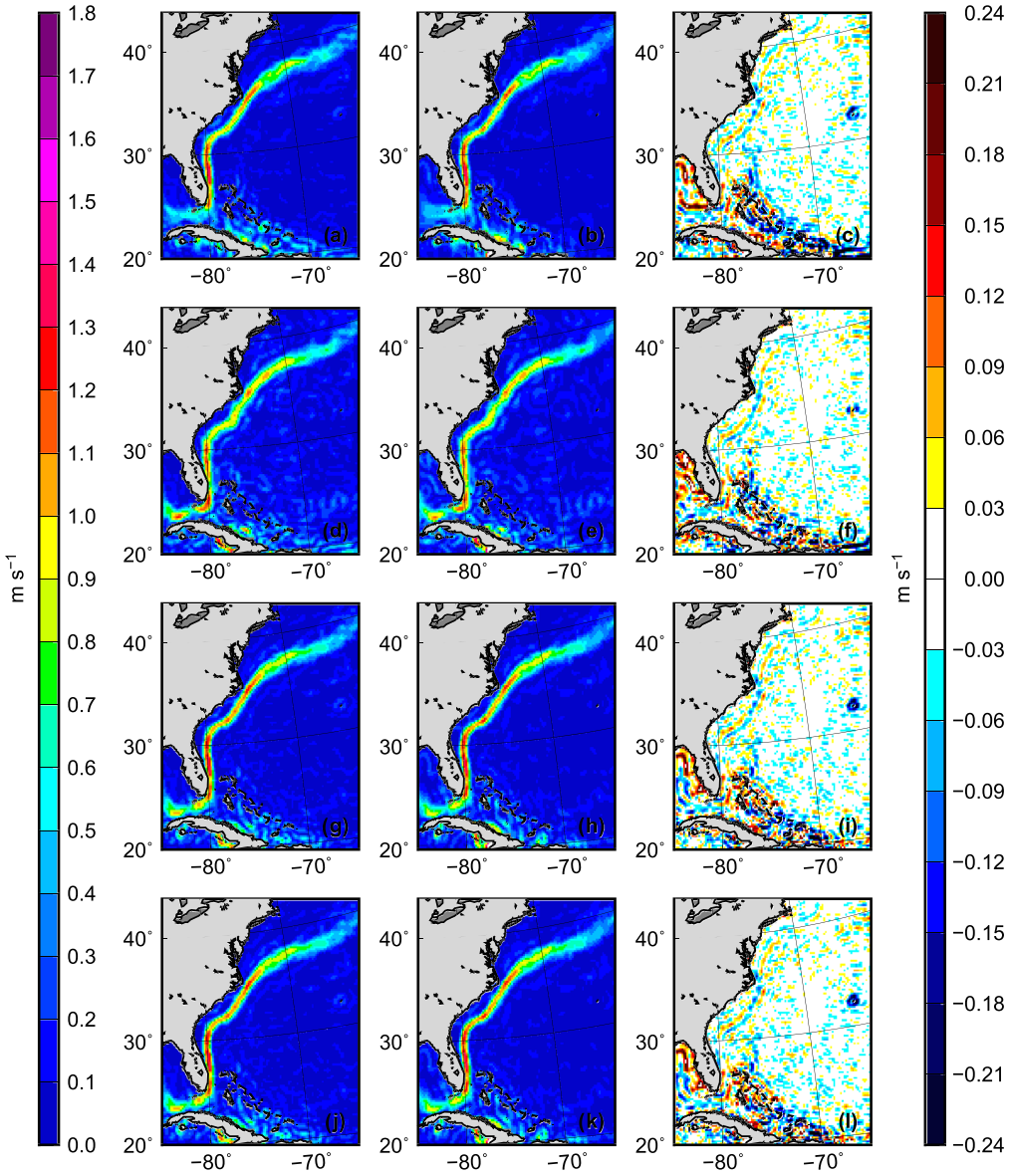

Figure 11. Absolute geostrophic surface currents (m s^{-1}) for the Gulf Stream region from geodetic MDTs applying (from top to bottom) EGM2008, Eigen6C4, GECO, and SGG-UGM-1 as geoid models for (left) maximum d/o 420, (middle) d/o 1,080, and (right) the difference (d/o 1,080 minus d/o 420). All MDT models are spatially filtered applying a truncated Gaussian kernel with 0.2 filter length.

methodology presented in this paper introduces the MDT as a global mathematical field with a continuous ocean-land transition and a smooth definition over land. To obtain an unambiguous global definition, the land mathematical values of the MDT are defined as the solution of the source-free heat equation with the coastal MDT as boundary condition. With this definition, any ocean MDT can be mathematically globalized and resolution can be reduced via subsequent SH analysis and synthesis. The land values of the MSS are consequently defined as sum of global MDT and geoid model. The coastal MDT values needed to solve the heat equation are obtained from MSS-geoid applying a high-resolution geoid model. The same geoid model is then added to the land MDT to obtain the final MSS values.

It is shown that the new methodology reduces strongly the MDT errors near the coast as well as the unphysical waves offshore. The often used approach to apply geoid height for land filling the MSS causes an ocean-land discontinuity from disregarding the coastal MDT. This discontinuity causes errors in the geodetic MDT which increase with decreasing resolution of the produced MDT. This feature is vanished with

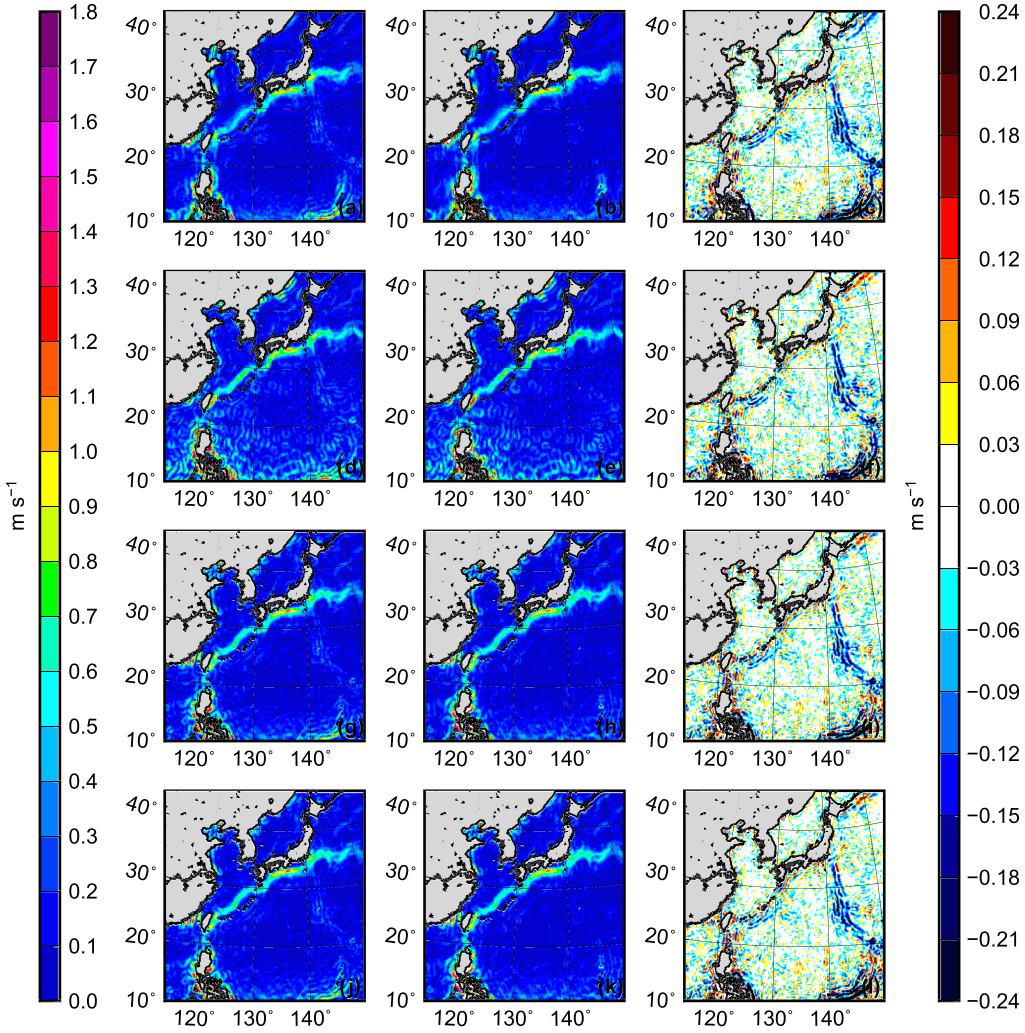

Figure 12. Same as Figure 9, but for the Kuroshio.

the new methodology as is shown by comparison with geostrophically corrected near-surface drifter velocities. Specifically for low maximum d/o, the geostrophic velocities from the MDTs fit now much better to the drifter data if the new method is applied. With the old method, an as high as possible resolution (with the applied geoid model) was generally necessary to minimize unphysical signals that are caused by both the ocean-land step and the ocean/land geoid spectral inconsistency and which grow with decreasing resolution. With this issue strongly diminished, the reduction in spatial resolution is a viable option to reduce the commission error in both geoid and MSS model increasing with spatial frequency.

To provide assistance for the choice of the MDT spatial resolution in practical applications, and as an interesting issue by itself, it is tested up to which maximum d/o physical signal is detectable in MDTs applying recent geoid models and DTU15 as MSS model. For two sections, one over the Gulf Stream and another one over the Kuroshio, the reconstruction of surface geostrophic velocities is investigated by comparison with drifter data and results of a high-resolution dynamic ocean model. Different resolutions up to maximum d/o 1,080 are tested. Specifically, increasing maximum velocity over the section is supposed as an indicator that small-scale information is added when resolution is increased. It is shown that all MDT models show increasing signal up to d/o 420 for both sections. Above this resolution, however, the evolution with increasing resolution is not clear. Strong geoid gradients exist close to both currents. Inconsistencies of MSS and geoid model seem to cause wavy structures that interfere with the currents generating spatial patterns depending on resolution.

However, a signal content at least up to d/o 420, which corresponds to a spatial scale of 48 km, lies well beyond the resolution of space-borne gravity observations. The source of the necessary short-scale information is not obvious. Over the ocean, the dominant data set to obtain short wave gravity information is satellite altimetry. A combined geoid model using satellite altimetry as input is thus distorted by the MDT included there (see e.g., Huang, 2017). It is not clear how much short-scale information remains in the geodetic MDT and how this depends on region and additional gravity data applied. For the western boundary currents discussed here, independent terrestrial gravity information might weigh down the influence of the altimetry data and allow for a better spatial resolution of small-scale currents than elsewhere. Fruitful discussions about this issue and in-depth investigations are necessary.

Appendix A: Laplacian Smoother

The Laplacian smoother as used in this paper allows a continuous and smooth land filling of global ocean gridded maps. A detailed description for solving Laplace's equation numerically is given, for example, by Hansen (1992). In this paper, Laplace's equation is solved for a global function ζ on a simple latitude-longitude map. Grid points are named (i,j), with $i = 1, \ldots, m$ and $j = 1, \ldots, n$ and $m(n)$ the number of rows (columns) of the grid. The set $\mathbb{M}$ contains all land grid points.

The four edges of the grid boxes define their direct neighbors that are used for the Laplacian smoothing. For the polar grid points $(1,j)$ and (m,j), only three neighbors are defined. The set $\mathbb{N}_{ij}$ contains the neighbors and n_{ij} the number of neighbors for grid point (i,j).

The approach is iterative. Before the iteration is started, all land points are set to zero, for example,

$$\zeta_{ij}^{0} = \begin{cases} 0 & \text{if} \quad (i,j) \in \mathbb{M} \\ \zeta_{ij} & \text{else} \end{cases} \tag{A1}$$

In each iteration step k, all land points obtain a new value according to

$$\zeta_{ij}^{k} = \begin{cases} \frac{1}{n_{ij}} \sum\limits_{(o,p)\in\mathbb{N}_{ij}} \zeta_{op}^{k-1} & \text{if } (i,j) \in \mathbb{M} \\ \zeta_{ij}^{k-1} & \text{else} \end{cases} \tag{A2}$$

The iteration is stopped if $\sum_{(i,j,)\in\mathbb{M}} |\zeta_{ij}^{k} - \zeta_{ij}^{k-1}| < \epsilon$, where ϵ is set to 10^{-6} m. The iteration works fine for the $10' \times 10'$ grid applied here. On finer grids, the procedure might be too slow, and it is recommended to downsample ζ to a coarser grid, do the iteration, and interpolate the obtained land values to the fine grid. With this approach, good initial land values are provided and a few iterations on the fine grid provide a smooth final solution.

Data Availability Statement

Computations needed to obtain geodetic MDTs were performed applying the GOCE User Toolbox (GUT) provided by the European Space Agency (ESA) and available at https://earth.esa.int/web/guest/software-tools/gut/about-gut/overview.

Acknowledgments
The sea level anomaly data used in this paper is provided by the Copernicus Marine Environment Monitoring Service (CMEMS). Support of the research was provided by the ESA funded project GOCE-OGMOC (Contract Change Notice No. 9 to Contract No. 18308/04/NL/MM). Thanks to Thomas Gruber and to two anonymous reviewers for their valuable comments and suggestions which helped greatly to improve the original manuscript. Open access funding enabled and organized by Projekt DEAL.

References

Albertella, A., & Rummel, R. (2009). On the spectral consistency of the altimetric ocean and geoid surface: A one-dimensional example. *Journal of Geodesy*, *83*(9), 805–815. https://doi.org/10.1007/s00190-008-0299-5

Andersen, O. B., Stenseng, L., Piccioni, G., & Knudsen, P. (2016). The DTU15 MSS (mean sea surface) and DTU15lat (lowest astronomical tide) reference surface. In *Esa living planet symposium 2016, prague, czech republic*.

Bingham, R. (2010). Nonlinear anisotropic diffusive filtering applied to the ocean's mean dynamic topography. *Remote Sensing Letters*, *1:4*, 205–212. https://doi.org/10.1080/01431161003743165

Bingham, R., Haines, K., & Hughes, C. W. (2008). Calculating the ocean's mean dynamic topography from a mean sea surface and a geoid. *Journal of Atmospheric and Oceanic Technology*, *25*(10), 1808–1822. https://doi.org/10.1175/2008JTECHO568.1

Biri, S., Serra, N., Scharffenberg, M. G., & Stammer, D. (2016). Atlantic sea surface height and velocity spectra inferred from satellite altimetry and a hierarchy of numerical simulations. *Journal of Geophysical Research: Oceans*, *121*, 4157–4177. https://doi.org/10.1002/2015JC011503

Boyer, T. P., Levitus, S., Garcia, H., Locarnini, R., Stephens, C., & Antonov, J. (2005). Objective analyses of annual, seasonal, and monthly temperature and salinity for the world ocean on a 0.25 grid. *International Journal of Climatology*, *25*(7), 931–945.

Brockmann, J. M., Zehentner, N., Hock, E., Pail, R., Loth, I., Mayer-Gurr, T., & Schuh, W. D. (2014). Egm_tim_rl05: An independent geoid with centimeter accuracy purely based on the GOCE mission. *Geophysical Research Letters*, *41*, 8089–8099. https://doi.org/10.1002/2014gl061904

Cunderlik, R., Mikula, K., & Tunega, M. (2013). Nonlinear diffusion filtering of data on the Earth's surface. *Journal of Geodesy*, *87*, 143–160. https://doi.org/10.1007/s00190-012-0587-y

Dee, D. P. (2011). The era-interim reanalysis: Configuration and performance of the data assimilation system. *Quarterly Journal of the Royal Meteorological Society*, *137*(656), 553–597. https://doi.org/10.1002/qj.828

Fecher, T., Pail, R., Gruber, T., & the GOCO consortium (2017). GOCO05c: A new combined gravity field model based on full normal equations and regionally varying weighting. *Surveys in Geophysics*, *38*(3), 571–590.

Feng, G., Jin, S., & Sanchez-Reales, J. M. (2013). Antarctic circumpolar current from satellite gravimetric models ITG-GRACE2010, GOCE-TIM3 and satellite altimetry. *Journal of Geodynamics*, *72*, 72–80.

Förste, C., Bruinsma, S. L., Abrikosov, O., Lemoine, J.-M., Marty, J. C., Flechtner, F., et al. (2014). Eigen-6c4 the latest combined global gravity field model including GOCE data up to degree and order 2190 of GFZ potsdam and GRGS toulouse. GFZ German Research Centre for Geosciences, https://doi.org/10.5880/ICGEM.2015.1

Gilardoni, M., Reguzzoni, M., & Sampietro, D. (2016). GECO: A global gravity model by locally combining GOCE data and EGM2008. *Studia Geophysica et Geodaetica*, *60*, 228–247.

Hansen, P. B. (1992). Numerical solution of Laplace's equation. (Electrical Engineering and Computer Science - Technical Reports). Syracuse Univesity, 168.

Huang, J. (2017). Determining coastal mean dynamic topography by geodetic methods. *Geophysical Research Letters*, *44*, 11,125–11,128. https://doi.org/10.1002/2017GL076020

Kalnay, Kanamitsu, M., Kistler, R., Collins, W., Deaven, D., Gandin, L., et al. (1996). The NCEP/NCAR 40-year reanalysis project. *Bulletin of the American Meteorological Society*, *77*, 437–470.

Knudsen, P., Bingham, R., Andersen, O., & Rio, M. H. (2011). A global mean dynamic topography and ocean circulation estimation using a preliminary GOCE gravity model. *Journal of Geodesy*, *85*, 861–879. https://doi.org/10.1007/s00190-011-0485-8

Liang, W., Xu, X., Li, J., & Zhu, G. (2018). The determination of an ultra high gravity field model SGG-UGM-1 by combining EGM2008 gravity anomaly and GOCE observation data. *Acta Geodaeticaet Cartographica Sinica*, *47*(4), 425–434. https://doi.org/10.11947/j.AGCS.2018.20170269

Lumpkin, R., & Johnson, G. C. (2013). Global ocean surface velocities from drifters: Mean, variance, El Niño-southern oscillation response, and seasonal cycle. *Journal of Geophysical Research: Oceans*, *118*, 2992–3006. https://doi.org/10.1002/jgrc.20210

Lumpkin, R., & Pazos, M. C. (2007). Measuring surface currents with surface velocity program drifters: The instrument, its data, and some recent results, *Lagrangian analysis and prediction of coastal and ocean dynamics* (pp. 39–67). Cambridge: Cambridge University Press.

Marshall, J., Hill, C., Perelman, L., & Adcroft, A. (1997). Hydrostatic, quasi-hydrostatic and nonhydrostatic ocean modelling. *Journal of Geophysical Research*, *102*, 5733–5752.

Maximenko, N. (2004). Correspondence between Lagrangian and Eulerian velocity statistics at the Asuka line. *Journal of Oceanography*, *60*, 681–687.

Pail, R., Fecher, T., Barnes, D., Factor, J. F., Holmes, S. A., Gruber, T., & Zingerle, P. (2018). Short note: The experimental geopotential model XGM2016. *Journal of Geodesy*, *92*(4), 443–451.

Pavlis, N. K., Holmes, S. A., Kenyon, S. C., & Factor, J. K. (2012). The development and evaluation of the Earth gravitational model 2008 (EGM2008). *Journal of Geophysical Research*, *117*, B04406. https://doi.org/10.1029/2011JB008916

Ralph, E. A., & Niiler, P. (1999). Wind-driven currents in the tropical pacific. *Journal of Physical Oceanography*, *29*, 2121–2129.

Rio, M.-H., & Hernandez, F. (2003). High-frequency response of wind-driven currents measured by drifting buoys and altimetry over the world ocean. *Journal of Geophysical Research*, *108*(C8), 3283. https://doi.org/10.1029/2002JC001655

Rummel, R., Balmino, G., Johannessen, J., Visser, P., & Woodworth, P. (2002). Dedicated gravity field missions—Principles and aims. *Journal of Geodynamics*, *33*(1–2), 3–20.

Sanchez-Reales, J. M., Andersen, O. B., & Vig, M. I. (2016). Improving surface geostrophic current from a GOCE-derived mean dynamic topography using edge-enhancing diffusion filtering. *Pure and Applied Geophysics*, *173*, 871–884. https://doi.org/10.1007/s00024-015-1050-9

Sanchez-Reales, J. M., Vigo, M. I., Jin, S., & Chao, B. (2013). Global surface geostrophic ocean currents derived from satellite altimetry and GOCE geoid. *Marine Geodesy*, *35*(S1), 175–189. https://doi.org/10.1080/01490419.2012.718696

Siegismund, F. (2013). Assessment of optimally filtered recent geodetic mean dynamic topographies. *Journal of Geophysical Research: Oceans*, *118*, 108–117. https://doi.org/10.1029/2012JC008149

Tapley, B. D., Bettadpur, S., Watkins, M. M., & Reigber, C. (2004). The gravity recovery and climate experiment: Mission overview and early results. *Geophysical Research Letters*, *31*, L09607. https://doi.org/10.1029/2004GL019920